



The Host Galaxies and Progenitors of Fast Radio Bursts Localized with the Australian Square Kilometre Array Pathfinder

Shivani Bhandari¹, Elaine M. Sadler^{1,2}, J. Xavier Prochaska^{3,4}, Sunil Simha³, Stuart D. Ryder⁵, Lachlan Marnoch^{1,5}, Keith W. Bannister¹, Jean-Pierre Macquart⁶, Chris Flynn⁷, Ryan M. Shannon⁷, Nicolas Tejos⁸, Felipe Corro-Guerra⁸, Cherie K. Day^{1,7}, Adam T. Deller⁷, Ron Ekers^{1,6}, Sebastian Lopez⁹, Elizabeth K. Mahony¹, Consuelo Nuñez⁸, and Chris Phillips¹

¹ Australia Telescope National Facility, CSIRO Astronomy and Space Science, P.O. Box 76, Epping NSW 1710, Australia; shivani.bhandari@csiro.au

² Sydney Institute for Astronomy, School of Physics A28, The University of Sydney, NSW 2006, Australia

³ University of California, Santa Cruz, 1156 High Street, Santa Cruz, CA 95064, USA

⁴ Kavli Institute for the Physics and Mathematics of the Universe (Kavli IPMU), 5-1-5 Kashiwanoha, Kashiwa, 277-8583, Japan

⁵ Department of Physics and Astronomy, Macquarie University, NSW 2109, Australia

⁶ International Centre for Radio Astronomy Research, Curtin University, Bentley WA 6102, Australia

⁷ Centre for Astrophysics and Supercomputing, Swinburne University of Technology, John Street, Hawthorn VIC 3122, Australia

⁸ Instituto de Física, Pontificia Universidad Católica de Valparaíso, Casilla 4059, Valparaíso, Chile

⁹ Departamento de Astronomía, Universidad de Chile, Casilla 36-D, Santiago, Chile

Received 2019 October 8; revised 2019 December 22; accepted 2019 December 23; published 2020 June 1

Abstract

The Australian SKA Pathfinder (ASKAP) telescope has started to localize fast radio bursts (FRBs) to arcsecond accuracy from the detection of a single pulse, allowing their host galaxies to be reliably identified. We discuss the global properties of the host galaxies of the first four FRBs localized by ASKAP, which lie in the redshift range $0.11 < z < 0.48$. All four are massive galaxies ($\log(M_*/M_\odot) \sim 9.4\text{--}10.4$) with modest star formation rates of up to $2 M_\odot \text{ yr}^{-1}$ —very different to the host galaxy of the first repeating FRB 121102, which is a dwarf galaxy with a high specific star formation rate. The FRBs localized by ASKAP typically lie in the outskirts of their host galaxies, which appears to rule out FRB progenitor models that invoke active galactic nuclei or free-floating cosmic strings. The stellar population seen in these host galaxies also disfavors models in which all FRBs arise from young magnetars produced by superluminous supernovae, as proposed for the progenitor of FRB 121102. A range of other progenitor models (including compact-object mergers and magnetars arising from normal core-collapse supernovae) remain plausible.

Unified Astronomy Thesaurus concepts: Galaxies (573); Radio continuum emission (1340); Radio bursts (1339); Star formation (1569)

1. Introduction

Fast radio bursts (FRBs) are bright, millisecond-scale duration radio emissions of unknown origin arising at cosmological distances (Cordes & Chatterjee 2019). Discovered by the Parkes radio telescope (Lorimer et al. 2007), the number of facilities around the world that have found FRBs has grown steadily in the last half-decade (Spitler et al. 2014; Masui et al. 2015; Bannister et al. 2017; Amiri et al. 2019; Farah et al. 2019; Ravi et al. 2019). Most recently, sensitive and wide field-of-view searches for FRBs have come online, and led to a significant increase in the discovery rate (Shannon et al. 2018; Amiri et al. 2019).

FRBs show extremely luminous coherent radiation of brightness temperature $T_b \sim 10^{35}$ K, whose $\sim 0.1\text{--}10$ ms duration confines their emission regions to $< 30\text{--}3000$ km. A wide range of theories have been advanced to account for these properties, from those involving supernovae in which the FRB is a feature of a young, expanding supernova remnant (SNR; Connor et al. 2016; Piro 2016) and superluminous supernovae (Metzger et al. 2017); the merger/collision of two compact objects such as binary neutron stars (NS–NS; Totani 2013; Yamasaki et al. 2018), binary white dwarfs (WD–WD; Kashiyama et al. 2013) and white dwarf–black hole mergers (WD–BH), the latter via the reconnection of magnetic material (Li et al. 2018); energetic activities from isolated compact objects such as giant pulses from extragalactic pulsars

(Cordes & Wasserman 2016); giant flares from magnetars (Popov & Postnov 2010; Pen & Connor 2015); collision/interaction of neutron stars with an active galactic nucleus (AGN; Vieyro et al. 2017) and NS “combing” (Zhang 2017); collapse of supramassive NSs (Falcke & Rezzolla 2014); superconducting cosmic strings (Cai et al. 2012; Zadorozhna 2015); and alien beams driving light sails (Lingam & Loeb 2017).

The localization of FRBs to host galaxies (HGs) will enable exploration of the host galaxy population, their global properties and local FRB environment, which is crucial in understanding FRB progenitor systems. The first localization was achieved for the first known “repeating FRB” 121102 (Spitler et al. 2016). It resides in a low-luminosity ($M_r \approx -17$), star-forming dwarf galaxy at a redshift of $z = 0.192$ (Chatterjee et al. 2017; Tendulkar et al. 2017). Its spatial coincidence with an active star-forming region in the host, a persistent high-luminosity radio source and an extreme magnetoionic environment led to a “concordance picture” of the source of FRB 121102 as a flaring magnetar embedded in a magnetized ion-electron wind nebula (Margalit & Metzger 2018).

Despite the recent discovery of the further repeating burst sources by the the Canadian Hydrogen Intensity Mapping Experiment telescope and the Australian Square Kilometre Array Pathfinder (ASKAP) (CHIME/FRB Collaboration et al. 2019; Kumar et al. 2019), the FRB population is still dominated by one-off and ostensibly non-repeating events.

They currently dominate statistical analyses of the FRB phenomenon, and they might have a different progenitor type and arise from cataclysmic implosions or mergers.

Recently, some of these one-off events from ASKAP (Bannister et al. 2019; Macquart et al. 2020; Prochaska et al. 2019) and the Deep Synoptic Array (DSA-10; Ravi et al. 2019; FRB 190523) have now been localized to Milky Way-like galaxies that are much more massive than the host galaxy of FRB 121102, suggesting that FRBs have diverse host galaxies.

The Commensal Real-Time ASKAP Fast Transients (CRAFT; Macquart et al. 2010) survey is the wide field-of-view FRB search program operating with ASKAP. Initially running in a fly’s-eye mode (in which multiple dishes are used, each pointing in different locations on the sky), the project found 25 FRBs¹⁰ with a range of dispersion measures (DMs), luminosities and widths in the latter half of 2018 (Shannon et al. 2018; Bhandari et al. 2019; Macquart et al. 2019; Qiu et al. 2019). Since late 2018, CRAFT has been operating the facility in incoherent-sum (ICS) mode, where all operating dishes are pointing to the same location and the signals are combined incoherently. FRBs detected in this way trigger a voltage download across all dishes that can be correlated and subarcsecond localizations of the FRB positions become possible.

In this Letter, we examine global properties of the host galaxies for the first four ASKAP-localized FRBs, namely FRB 180924, FRB 181112, FRB 190102, and FRB 190608. In Section 2, we describe the optical follow-up observations and the derived host galaxy properties. Section 3 presents their radio follow-up observations and properties. Section 4 discusses the comparison of the properties with other localized FRBs along with FRB models that are ruled out (or favored) by our observations and results. We conclude and provide a summary of our findings in Section 5.

2. Optical Properties of the Host Galaxies of ASKAP FRBs

Between 2018 September and 2019 June, four FRBs were localized with ASKAP, each of which was unambiguously associated to a host galaxy. Each burst fell within 1'' of an $r < 22$ mag galaxy, with an estimated chance localization of only $\approx 0.3\%$ for a single object (Prochaska et al. 2019), or $\approx 10^{-10}$ for the combined set. Survey and targeted follow-up imaging and spectroscopy data in optical and near-infrared (near-IR) passbands were collected to measure the redshifts and other properties of the host galaxies.

Although public imaging survey data such as from the Dark Energy Survey (DES; Abbott et al. 2018) and Sloan Digital Sky Survey (SDSS; Blanton et al. 2017) were available for most host galaxies, additional follow-up imaging was conducted using the FOcal Reducer/low dispersion Spectrograph 2 (FORS2; Appenzeller et al. 1998), X-shooter (Vernet et al. 2011) mounted on the European Southern Observatory’s Very Large Telescope (VLT) and Sinistro¹¹ instrument mounted on a 1 m telescope at the Las Cumbres Observatory (LCOGT; Brown et al. 2013). Optical spectroscopy of the host galaxies was conducted using the Keck Cosmic Web Imager instrument (KCWI; Morrissey et al. 2018) on the W. M. Keck telescope; the Gemini Multi-Object Spectrograph (GMOS; Hook et al. 2004) mounted on the Gemini-South telescope; FORS2 at the

VLT; and the *Magellan* Echellette spectrograph (Marshall et al. 2008, MagE) on the *Magellan* Baade telescope.

We derived properties for each of the host galaxies such as stellar mass, star formation rate (SFR), internal extinction, and colors from the optical data (see Table 1). VLT imaging was reduced with ESOREFLEX (Freudling et al. 2013) or CCDPROC (Craig et al. 2017), individual frames were co-added with MONTAGE (Jacob et al. 2010) and photometry was performed using SEXTRACTOR (Bertin & Arnouts 1996), as described in Prochaska et al. (2019). We corrected for Galactic extinction using the Schlafly & Finkbeiner (2011) law and interpolation of extinction values using the IRSA Dust tool.¹² We then used the CIGALE package (Noll et al. 2009) to perform spectral energy distribution (SED) fits of the data to obtain the aforementioned galaxy properties. The spectra were analyzed with the pPXF package (Cappellari 2017) to measure nebular line ratios and draw inferences on excitation state of the gas. Bannister et al. (2019), Prochaska et al. (2019), and Macquart et al. (2020) give the full details of the procedure, and the complete data set of measurements and derived quantities are available in the GitHub FRB repository.¹³

Table 1 lists a range of measured and derived properties for the ASKAP FRBs, as well as for the only two other (known to date) localized FRBs: 121102 (Chatterjee et al. 2017) and 190523 (Ravi et al. 2019). We now briefly summarize relevant aspects of each ASKAP FRB host galaxy.

2.1. FRB 180924

FRB 180924 was detected on 2018 September 24 at UT 16:23:12 and has a DM of $362.4 \pm 0.2 \text{ pc cm}^{-3}$. It was localized to a luminous, quiescent galaxy, DES J214425.25–405400.81 at a redshift of $z = 0.3214$ based on well-detected [O II], [O III], H α , H β emission and stellar Ca H + K absorption spectral lines using the KCWI and Gemini-S/GMOS spectrograph. The [O III] and high [N II]/H α flux ratio indicate low-ionization narrow emission-line region (LINER) emission (Yan & Blanton 2012). A detailed description of the follow-up observations and properties of the host galaxy of FRB 180924 is given in Bannister et al. (2019).

Analysis of the Multi Unit Spectroscopic Explorer (MUSE; Bacon et al. 2010) data from the VLT obtained on 2018 November 5 UT shows that the ionized gas is distributed throughout the host galaxy, including at the position of FRB 180924. The H α emission-line flux at the burst position is similar to the average H α emission at the same radius in the host, so the spectroscopic data show no evidence for any enhanced star formation at the position of the FRB, although we are spatially limited by the seeing of the observations, with effective point-spread function of $0''.8$.

2.2. FRB 181112

FRB 181112 was detected on 2018 November 12 at UT 17:31:15 and has a DM of $589.0 \pm 0.3 \text{ pc cm}^{-3}$. It is associated with the galaxy DES J214923.66–25815.28. On UT 2018 December 5, observations of the host of FRB 181112 with the VLT/FORS2 spectrograph established the redshift of the galaxy to be $z = 0.4755$ from nebular emission lines such as [O III], [N II], H α and H β indicating ongoing star formation.

¹⁰ An additional burst was found in offline ICS search (Agarwal et al. 2019).

¹¹ <https://lco.global/observatory/telescopes/1m/>

¹² <https://irsa.ipac.caltech.edu/applications/DUST/>

¹³ <https://github.com/FRBs/FRB>

Table 1
Comparison of the Properties of the ASKAP FRB Host Galaxies with the Host Galaxies of FRB 121102 and FRB 190523

Properties	FRB 121102 Tendulkar et al. (2017)	FRB 190523 Ravi et al. (2019)	FRB 180924 Bannister et al. (2019)	FRB181112 Prochaska et al. (2019)	FRB 190102 Macquart et al. (2020)	FRB 190608 Macquart et al. (2020)
Detection telescope	Arecibo	DSA-10	ASKAP-ICS	ASKAP-ICS	ASKAP-ICS	ASKAP-ICS
<i>FRB</i>						
DM (pc cm ⁻³)	557(2)	760.8(6)	362.4(2)	589.0(3)	364.5(3)	339.5(5)
DM _{ISM} NE2001 (pc cm ⁻³)	188.0	37.0	40.5	40.2	57.3	37.2
R.A. (J2000)	05 ^h 31 ^m 58 ^s .698(8)	13 ^h 48 ^m 15 ^s .6(2)	21 ^h 44 ^m 25 ^s .255(8)	21 ^h 49 ^m 23 ^s .63(24)	21 ^h 29 ^m 39 ^s .76(17)	22 ^h 16 ^m 4 ^s .74(3)
Decl. (J2000)	+33 ^d 08′52″.6(1)	+72 ^d 28′11(2)″	-40 ^d 54′00″.1(1)	-52 ^d 58′15″.4(14)	-79 ^d 28′32″.5(6)	-07 ^d 53′53″.6(4)
Rotation measure (RM; rad m ⁻²)	~10 ⁵	...	14	10	110	...
Fluence (Jy ms)	>0.1	280	16(1)	26(3)	14(1)	26(4)
Pulse width (ms)	3.0(5)	0.42(5)	1.76(9)	2.1(2)	1.7(1)	6.0(8)
Energy ^a (erg Hz ⁻¹)	3.7 × 10 ²⁹	5.6 × 10 ³³	3.5 × 10 ³¹	1.0 × 10 ³²	2.3 × 10 ³¹	7.6 × 10 ³⁰
<i>Host galaxy</i>						
Redshift	0.19273(8)	0.660(2)	0.3214(2)	0.4755(2)	0.2913(2)	0.11778
<i>u</i> - <i>r</i> (rest frame) ^b	...	1.95	1.75(16)	1.15(15)	1.33(22)	1.49(11)
<i>M</i> _r (rest frame)	-17.0(2)	-22.05(12)	-20.76(5)	-20.34(7)	-19.90(7)	-21.15(5)
Galactic <i>E(B - V)</i> ^c	0.0165	0.0174	0.1994	...
log stellar mass (<i>M</i> _⊙)	7.6-7.8	11.07(6)	10.35(14)	9.42(20)	9.50(35)	10.40(14)
SFR ^d (<i>M</i> _⊙ yr ⁻¹)	0.4	<1.3(2)	<2	0.6	1.5	1.2
log sSFR (yr ⁻¹)	-8.14	<-10.95	<-10.0	-9.62	-9.33	-10.30
Metallicity <i>Z</i>	0.008(10)	0.006(12)	0.011(16)	0.009(14)
Projected offset from galaxy center (kpc)	3.5(9)	3.1 ^{+15.7} _{-3.1}	1.5 ^{+3.4} _{-1.5}	6.8(13)
Half-light radius (kpc)	2.5(3)	8(3)	5.3(1)	NA ^e
log <i>S</i> _{radio} (6.5 GHz, W Hz ⁻¹)	22.27	...	<21.73	<22.11	<21.62	<20.55
<i>F</i> _{radio} (6.5 GHz, μJy)	~200	...	<21	<21	<19	<10.5

Notes.

^a The energies are derived assuming a flat spectrum for FRBs ($\alpha = 0$) and zero k-correction.

^b Rest frame colors are derived using CIGALE.

^c Galactic reddening values along host galaxy lines of sight estimated using the Schlafly & Finkbeiner (2011) extinction law and the IRSA dust tool.

^d Derived from the dust-corrected H α luminosity using the standard scaling law. Uncertainties are dominated by systematic errors, e.g., dust correction, aperture losses, which may be as high as 50%.

^e Half-light radius derived from GALFIT is not a true representation because of the complex galaxy structure.

See Prochaska et al. (2019) for further details of this host galaxy, and a foreground galaxy whose halo was intersected by the FRB.

2.3. FRB 190102

FRB 190102 was detected on 2019 January 2 at UT 05:38:43 and has a DM of 364.5 ± 0.3 pc cm⁻³ (Macquart et al. 2020). A host was identified in deep FORS2 imaging performed in *g* and *I* band with the VLT on 2019 January 12 UT.

On UT 2019 March 12, we observed the host galaxy with the *Magellan*/MagE spectrograph and obtained a redshift of $z = 0.29$ from the [O II] doublet (resolved) and other nebular emission lines, which was also confirmed in our VLT/FORS2 spectrograph observations on 2019 March 25, from H α emission. Its photometry and nebular line emission indicate a star-forming galaxy with a modest SFR and stellar mass (Table 1).

2.4. FRB 190608

FRB 190608 was detected on 2019 June 8 at UT 22:48:12 and has a DM of 339.5 ± 0.5 pc cm⁻³ (Macquart et al. 2020). It was localized to the star-forming galaxy SDSS J221604.90-075355.9

at a redshift $z = 0.118$, obtained from SDSS data release 9 (Ahn et al. 2012). This is a relatively well-studied galaxy, which is known to host a Type 1 (broad-line) AGN (Stern & Laor 2012). Our derived SFR for this galaxy ($1.24 M_{\odot} \text{ yr}^{-1}$, as listed in Table 1) agrees reasonably well with the SDSS DR12 (Alam et al. 2015) value of $1.7 \pm 0.2 M_{\odot} \text{ yr}^{-1}$.

On UT 2019 August 21, we performed deep *g*-band imaging of this host with the X-shooter instrument at the VLT. These observations show spiral arms that were too faint to be observed in the SDSS data. Figure 1 shows an image of this and the other host galaxies.

2.5. Potential Biases in FRB Detection

There are features in FRB search algorithms that can bias their detection. The detectability of an FRB is a complex function of the FRB fluence, the pulse profile, and the DM. The detectability declines with increasing DM due to “DM smearing.” Intrinsic pulse width will also reduce the signal to noise of the burst below the triggering threshold (Connor 2019).

The limits on both DM and fluence will bias against high- z FRB events and we recognize that the sample studied here only reflects the $z < 0.5$ FRB population. Also, the observed FRBs

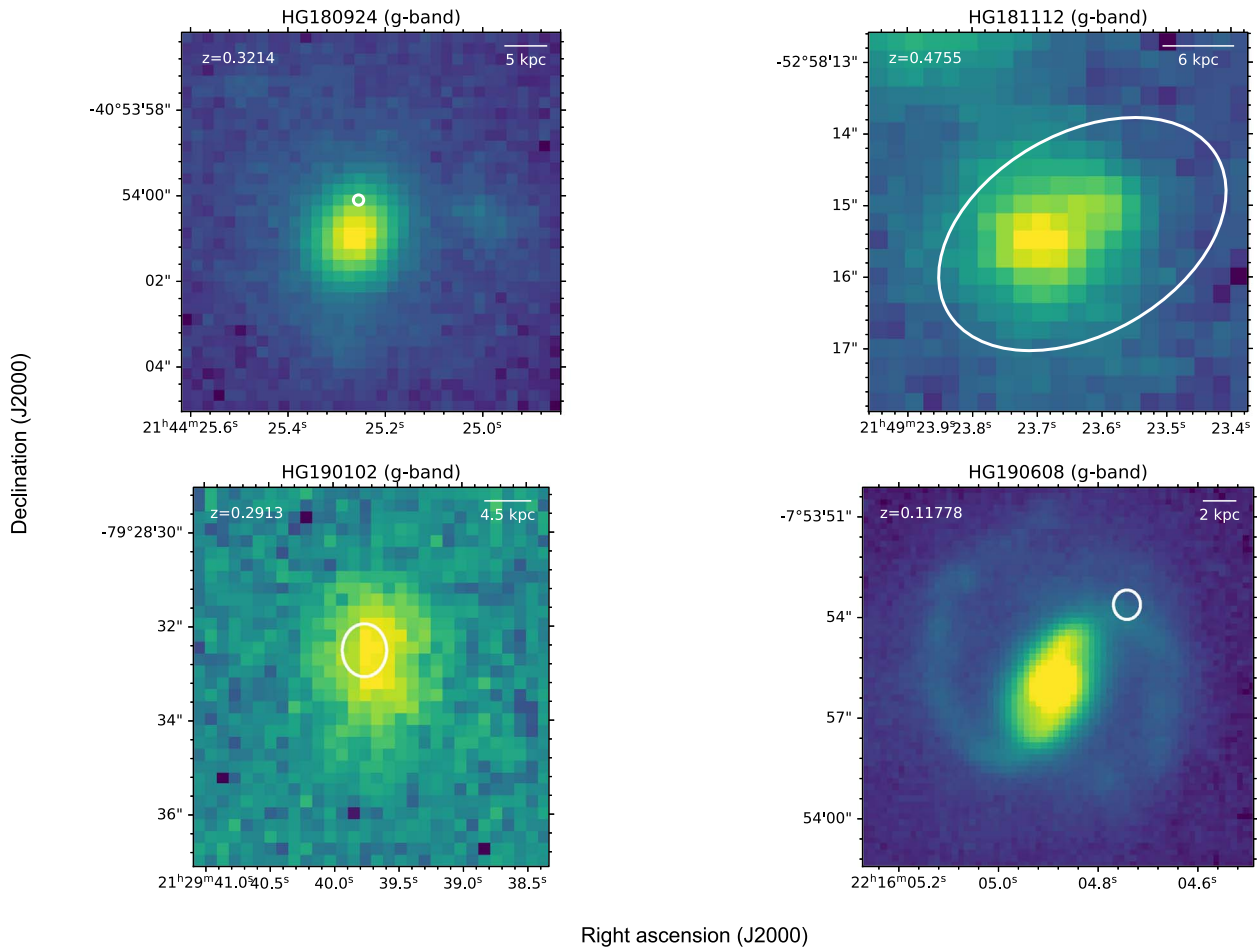


Figure 1. *g*-band FORS2/X-Shooter images of the host galaxies for a sample of localized FRBs (FRB 180924, FRB 181112, FRB 190102, and FRB 190608), overlotted with the positions of each FRB. The white circle/ellipse represents the total uncertainty in the FRB position.

may be biased against occurring in highly turbulent environments (e.g., active star-forming regions) where the signal would be temporally broadened by scattering (Macquart & Johnston 2015).

3. Radio Continuum Properties of the ASKAP FRB Host Galaxies

We searched for persistent radio continuum emission from the host galaxies of FRB 180924, FRB 181112, FRB 190102, and FRB 190608 using the Australia Telescope Compact Array (ATCA; project code C3211). The observations were triggered within 10 days of the burst and were conducted in the 4 cm band, with center frequencies at 5.5 and 7.5 GHz, using the ATCA’s highest resolution array configurations. We observed a single epoch for FRB 180924, FRB 181112, and FRB 190608 and two epochs for FRB 190102 (see the Appendix, Table 4). We combined the data from the two IF bands, and also combined the two epochs for FRB 190102, to perform a deep search of radio continuum emission at 6.5 GHz from the position of the FRB host galaxies.

We found no continuum emission from anywhere within the host galaxies of FRB 180924, FRB 181112, or FRB 190102 above a $\sim 20 \mu\text{Jy}$ flux density limit (3σ). However, potentially resolved emission of $\sim 65 \mu\text{Jy}$ was observed at 5.5 GHz with a NS–EW resolution of $20'' \times 2''$ from the host of FRB 190608. No radio emission was observed at 7.5 GHz above our $45 \mu\text{Jy}$

flux density limit (3σ) for the field of FRB 190608. The detection at 5.5 GHz was not very significant and therefore we triggered the Jansky Very Large Array (JVLA) at UT 2019 August 28 in the band spanning between 4 and 8 GHz for deeper observations (project code 19A-121). The observations were taken in the most extended “A” configuration of the JVLA, with a resolution of ~ 0.4 arcseconds using natural weighting. We detected resolved radio continuum emission (estimated size $\sim 2''5$) with a peak brightness of $16 \mu\text{Jy beam}^{-1}$ (4.5σ significance), coincident with the nucleus of the host galaxy. Tapering the synthesised beam to a circular Gaussian with FWHM of $0''8$ increased the detection significance to 6σ , with a peak brightness of $\sim 27 \mu\text{Jy beam}^{-1}$. The discrepancy between the JVLA and ATCA brightness measurements suggests that some emission is still resolved out by the JVLA observations.

The diffuse nature and probable steep spectrum of the emission suggest that this is synchrotron emission due to star formation in the host galaxy. Because we know that several of the host galaxies of our ASKAP FRBs have ongoing star formation, we can estimate the level of radio continuum emission expected from star formation alone. For this, we assume a radio-SFR relation at 1.4 GHz of $\log P_{1.4} = \log \text{SFR} + 20.95$ (Sullivan et al. 2001) where P is the radio luminosity. With the exception of FRB 190608, the star formation contribution to the radio continuum emission at 6.5 GHz is expected to be less than $1\text{--}2 \mu\text{Jy}$. For the closest host galaxy

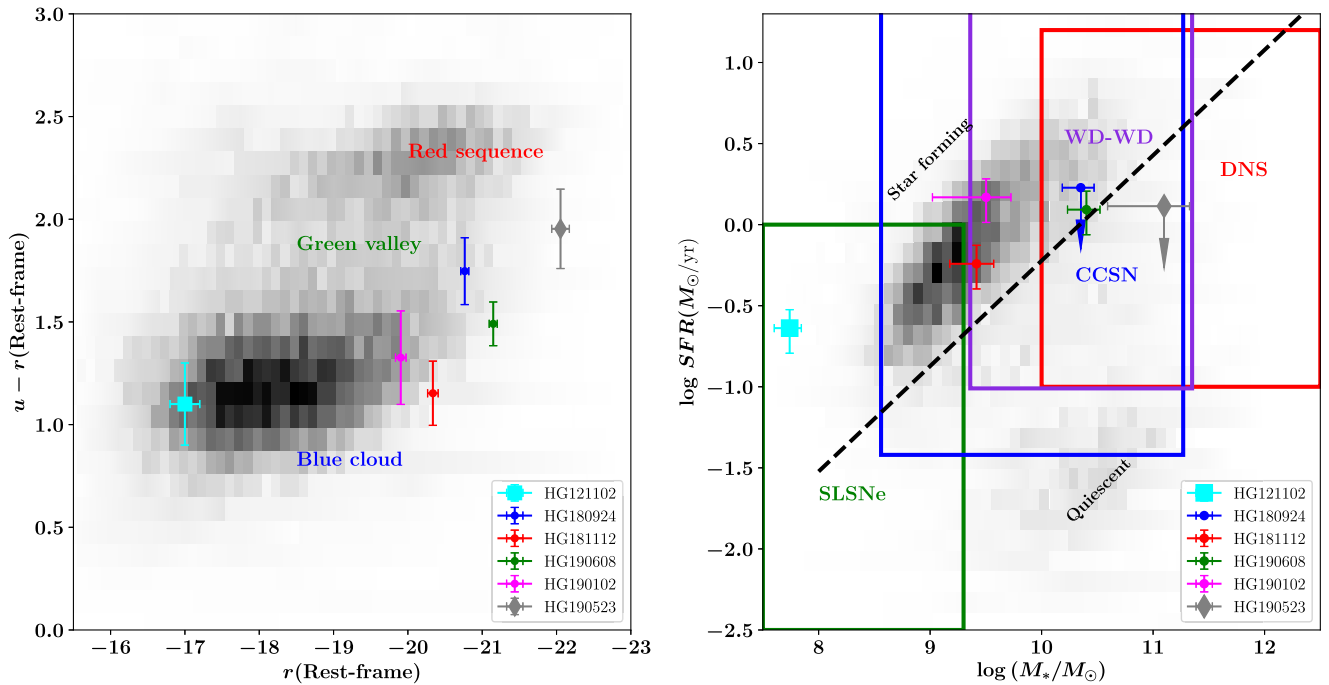


Figure 2. Left panel: rest-frame color–magnitude diagram of the host galaxies (HGs) of the repeater (FRB 121102), FRB 190523, and ASKAP FRBs compared to the population of $z \sim 0.3$ galaxies taken from the PRIMUS survey (Moustakas et al. 2013). Note that the $u-r$ color for FRB 121102 is a notional value based on its star-forming properties. Right panel: distribution of SFR vs. stellar mass for PRIMUS galaxies at $z \sim 0.3$ compared against values for the host galaxies of repeater, FRB 190523, and ASKAP FRBs. Upper limits on SFR are plotted for the hosts of FRB 180924 and FRB 190523. The dashed line separates the primary sequences of star-forming and quiescent galaxies. The green box boundary represents the 90% region populated by the hosts of superluminous supernovae (Perley et al. 2016). The blue and violet boundaries represent the 90% region of the galaxies hosting CCSNe and WD mergers, respectively (Kelly & Kirshner 2012; Wolf et al. 2016), whereas the red boundary represents the simulated galaxies that are likely to host DNS with merger rate $>10^4$ per galaxy per Gyr as presented in Artale et al. (2019).

(FRB 190608), the expected contribution is $\sim 10 \mu\text{Jy}$ for a SFR of $\sim 1 M_{\odot} \text{ yr}^{-1}$ (assuming a radio spectral index of -0.7), which within the uncertainties, is consistent with our observations.

The 3σ limits on radio continuum luminosity from a compact source at the locations for all four ASKAP FRBs are presented in Table 1. These limits are lower than the luminosity of the FRB 121102 persistent source ($L = 1.8 \times 10^{22} \text{ W Hz}^{-1}$), indicating that the bursts originate from less extreme environments, if they have the same progenitors as the repeating FRB. From these data, we conclude that none of the four ASKAP FRB host galaxies contains a persistent compact radio source as intrinsically luminous as that seen in the host galaxy of FRB 121102. Deeper continuum searches, particularly at frequencies of a few GHz, are feasible and will provide more stringent limits or a possible detection.

4. Discussion

4.1. Comparison of the ASKAP FRB Host Galaxies with the General Galaxy Population at $z \sim 0.3$

We can place the ASKAP FRB hosts in context with the cosmic population by comparing their properties with a representative set of galaxies at similar redshifts. In Figure 2, we compare the color–magnitude and SFR–stellar mass (M_*) distributions of the FRB host galaxies with those of the general population of galaxies at redshift $z \sim 0.3$ from the PRIMUS survey (Moustakas et al. 2013).

The left panel (color–magnitude) of Figure 2 provides some information about the overall stellar population in these galaxies. The host galaxies of the ASKAP FRBs lie toward the bright end of the magnitude distribution, and mainly near

the star-forming “blue cloud” (Strateva et al. 2001)—though the FRB 180924 host galaxy lies in the more sparsely populated “green valley” region where galaxies are expected to be transitioning between star-forming and quiescent systems (Martin et al. 2007). Although the ASKAP FRB hosts are relatively massive galaxies, none of them lie in the “red and dead” zone.

The right panel of Figure 2 shows the current SFR as a function of galaxy stellar mass. The four ASKAP FRB host galaxies all have stellar masses above a few times $10^9 M_{\odot}$, and their SFRs mainly lie on or below the star-forming main sequence for galaxies of this stellar mass—i.e., none of these objects are “starburst” galaxies (with $\text{sSFR} > -8.7$), and only one (FRB 180924) is potentially “quiescent.”

4.2. Constraints on Progenitor Models from the HG Properties of ASKAP FRBs

Table 2 lists some of the main FRB progenitor models, based on information from the literature as summarized by Platts et al. (2018).

The localization of ASKAP FRBs (particularly FRB 180924 and FRB 190608) to the outskirts of their HGs show (i) that FRBs indeed come from galaxies, and (ii) that they are typically not coincident with the nucleus of their hosts. This information already appears to disfavor a range of models involving AGN, supermassive black holes and superconducting cosmic strings.

In Table 2, we separate progenitors that are expected to arise exclusively from a young (<10 – 100 Myr) stellar population from those that can also arise from old or intermediate-age stellar populations. Although the sample of localized FRBs is

Table 2
Some Popular FRB Progenitor Models, and the Stellar Populations from which they Arise

	<i>Young Stellar Population</i> (age <10–100 Myr)	<i>General Stellar Population</i> (all ages)	<i>Non-stellar Models</i>
<i>Cataclysmic</i> (single burst)	<i>Supernovae:</i> Core-collapse SN (CCSN) SLSN/long GRB	<i>Compact-object mergers:</i> NS–NS merger (DNS) WD–WD merger NS–BH merger BH–BH merger	
<i>Episodic</i> (potential for repeat bursts)	<i>Magnetars:</i> Young magnetar from SLSN Magnetar from CCSN <i>Pulsars:</i> Pulsar giant flares Young SNR pulsars	<i>Magnetars:</i> Magnetar from DNS merger <i>White dwarfs:</i> WD from WD–WD mergers White dwarf collapse (AIC) NS–WD accretion	<i>Supermassive black holes:</i> AGN outburst NS interaction with AGN <i>Other:</i> Superconducting cosmic strings

Note. The information in this table is drawn from the much larger compilation of FRB progenitor models published by Platts et al. (2018).

still small, this approach allows us to start addressing some general questions about FRB progenitors.

If FRBs arise mainly from “young stellar population” progenitors, we would expect them to occur mainly in the kinds of HGs where most stars are currently forming. These are typically massive galaxies with stellar masses 10^{10} – $10^{11} M_{\odot}$ and SFR $>1 M_{\odot} \text{ yr}^{-1}$ (Brinchmann et al. 2004).

In contrast, if most FRBs progenitors come mainly from an old or intermediate-age stellar population (e.g., merging NSs), then they should mainly occur in the kinds of massive galaxies where most stars (of all ages) lie. These are typically galaxies with stellar masses above $10^{10} M_{\odot}$, with a wider range in current SFR.

We now explore the expected location in the stellar mass–SFR plot (right-hand plot in Figure 2) of the host galaxies of FRBs that arise from two possible progenitor channels: (i) cataclysmic events associated with the mergers of compact objects (NSs, WDs, or stellar-mass black holes), and (ii) potentially repeating bursts from young magnetars, which may be produced from the explosion of superluminous supernovae (SLSNe), from core-collapse supernovae (CCSNe), or potentially from the merger of two neutron stars or white dwarfs (NS–NS, see Margalit et al. 2019; WD–WD mergers, see Levan et al. 2006).

HGs of NS, WD, or BH merger events: recent simulations (Artale et al. 2019) predict that 70% of simulated NS–NS mergers, 55% of BH–NS mergers, and 53% of BH–BH mergers occur in galaxies with stellar mass $>10^{10} M_{\odot}$ and SFR $>0.1 M_{\odot} \text{ yr}^{-1}$ (as shown by the red-bordered region of the right plot in Figure 2).

We find that 2/4 of ASKAP FRB hosts (and 3/5 of the localized, one-off FRB hosts in Table 1) lie in a similar range of stellar mass and SFR. We take type Ia supernova (which are believed to arise from WD–WD mergers or a single-degenerate scenario) as a proxy for all binary WD mergers. According to Wolf et al. (2016), 90% of the host galaxies of SNe Ia lie within the violet-bordered “WD–WD” merger region of Figure 2, in which all four of the ASKAP FRB host galaxies also lie.

HGs of young magnetars from SLSNe: high-energy transients such as SLSNe and long gamma-ray bursts are preferentially hosted by low-mass, and high SFR dwarf galaxies (Fruchter et al. 2006)—similar to the host of FRB 121102. Observations of low-redshift SLSNe (Perley et al. 2016) show that over 90% of them arise in galaxies that

have stellar mass $<2 \times 10^9 M_{\odot}$ and lie close to the star formation main sequence. As can be seen from Figure 2, none of the ASKAP FRB host galaxies lie in the region where most SLSNe hosts are found.

HGs of young magnetars from CCSNe: young magnetars can also be produced by the much larger population of regular CCSNe. According to Kelly & Kirshner (2012), 90% of the host galaxies of CCSNe, which are mostly massive with $\log M_{*}/M_{\odot} >9.5$, lie within the blue-bordered “CCSN” region in Figure 2, and all four of the ASKAP FRB host galaxies also lie in this region. As the FRB samples grow, potential biases in CCSNe selection may become important in the near future.

From Figure 2, we conclude that models in which all FRBs come from SLSNe/long GRB progenitors appear highly unlikely. The host galaxies of the four localized ASKAP FRBs in Table 1 are all “normal” massive galaxies of the kind that would be expected if most FRBs come from the general stellar population.

From host galaxy considerations alone, several FRB progenitor models still appear plausible: (i) magnetars from CCSNe; (ii) magnetars from NS–NS mergers (Margalit et al. 2019) or WD–WD mergers (Levan et al. 2006); (iii) cataclysmic FRBs from NS–NS mergers, WD mergers, WD accretion mechanisms, BH mergers or a combination of these.

4.3. Energy Range of the ASKAP FRBs

As can be seen from Table 1 and Figure 3, the localized ASKAP FRBs fall within the energy range (2×10^{30} to $2 \times 10^{34} \text{ erg Hz}^{-1}$) spanned by the ASKAP and Parkes FRBs studied by Shannon et al. (2018). Any conclusions that we can draw about the nature of the HGs and progenitors of these localized bursts should therefore be applicable to the general population of FRBs within this energy range, but cannot necessarily be extrapolated to any population of weaker bursts with energies below about $2 \times 10^{30} \text{ erg Hz}^{-1}$.

4.4. Is the HG of FRB 121102 Atypical?

Our analysis of the properties of ASKAP-localized FRBs and their hosts has shown that the repeating source FRB 121102 is anomalous. It is different in its energetics and polarization properties as compared to the ASKAP FRB population. The energies of most of the published repeating bursts from the source of FRB 121102 are 10–100 times lower

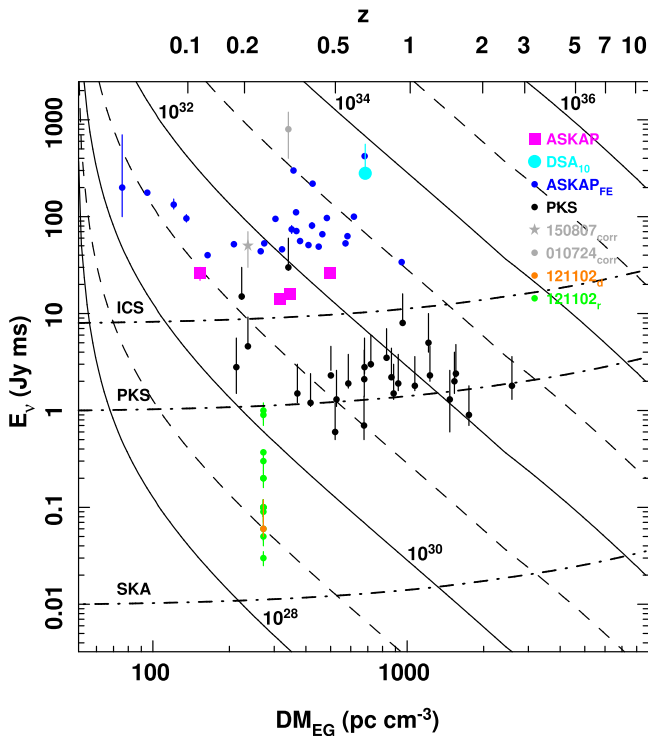


Figure 3. Distribution of fluences and energies for FRBs detected in the fly’s eye survey with ASKAP (blue data points), with the Parkes radio telescope (black data points), beam-corrected fluences for two Parkes FRBs (gray data points), FRB 190523 detected with DSA-10 (cyan data point), and repeating bursts detected from FRB 121102 (original burst in orange and repeating bursts in green); adapted from Figure 2 of Shannon et al. (2018). Magenta data points are the sample of localized ASKAP FRBs detected in incoherent searches. The black curves show contours of constant spectral energy density, in units of erg Hz^{-1} . The upper horizontal axis shows the redshift assuming a homogeneously distributed intergalactic plasma, and a host contribution to the DM of $50(1+z)^{-1} \text{pc cm}^{-3}$ (Shannon et al. 2018). Non-localized FRBs are plotted based on their excess DM using the lower horizontal axis, while localized FRBs are plotted based on their spectroscopic redshifts and the upper horizontal axis.

than any of the ASKAP FRBs. The RM observed for FRB 121102 is 1000 times higher than for any of the ASKAP FRBs, suggesting an unusual (or at least atypical) environment for this repeating FRB. In terms of the radio properties of HGs, none of the ASKAP HGs have a compact persistent radio source as luminous as the one in the FRB 121102 host galaxy, despite the ASKAP bursts being at least 100 times more energetic.

The HG for FRB 121102 is a low-mass dwarf and has an elevated SFR for its stellar mass. As Bannister et al. (2019) pointed out (their Table S8), fewer than 1% of stars lie in galaxies as faint as this. As the nature of the ASKAP FRB hosts implies that most FRBs are drawn from the general stellar population, the location of an FRB in such a small galaxy is (in hindsight) surprising.

Lastly, the ASKAP bursts have not been seen to repeat at the rate observed for FRB 121102 (James 2019). It seems very unlikely that FRB 121102 is drawn from the same population as the ASKAP FRBs.

4.5. Next Steps and Future Work

The sample of four localized FRBs has enabled us to study the global properties of their host galaxies. A direct measurement of the ionized missing baryons along the line of sight of

these FRBs is also performed in Macquart et al. (2020). At least arcsecond level localization, as demonstrated by ASKAP FRBs, is required not only for confident HG associations but also to study FRB environments using deep integral field unit (IFU) and imaging observations. A much larger sample of the host galaxies for FRBs is required to better characterize the host galaxy population and the distribution of FRBs within the host galaxies.

5. Conclusions

The galaxy colors and SFRs of the HGs of ASKAP FRBs show a diversity of properties and are not confined in a well-defined locus of a particular class. They exhibit lower star formation relative to their high stellar mass, very different to the host of FRB 121102, which is a starburst dwarf galaxy. Additionally, no persistent co-located compact radio sources were detected at the level seen in the host of FRB 121102.

The arcsecond localization of most ASKAP FRBs, and subarcsecond localization of FRB 180924, confirms that they occur in the outer regions of their hosts, ruling out the models involving AGNs and superconducting cosmic strings for all FRBs.

The global properties of the host galaxies of ASKAP FRBs suggest that the broader population of FRBs can arise from both young and (moderately) old progenitors. The considerations of the HG properties make SLSNe less likely to be their progenitors, while WD–WD and NS–NS mergers, accretion-induced WD collapse and regular CCSNe seem to be plausible mechanisms for at least a subset of the FRB population.

Based on observations collected at the European Southern Observatory under ESO programmes 0102.A-0450(A) and 0103.A-0101(B). K.W.B., J.P.M., and R.M.S. acknowledge Australian Research Council (ARC) grant DP180100857 A.T.D. is the recipient of an ARC Future Fellowship (FT150100415). S.O. and R.M.S. acknowledge ARC grant FL150100148. R.M.S. also acknowledges support through ARC grant CE170100004. N.T. and F.C.G. acknowledges support from PUCV/VRIEA project 039.395/2019. S.L. was funded by projects UCh/VID-ENL18/18 and FONDECYT 1191232. J.X.P. and S.S. are supported by NSF AST-1911140. The Australian Square Kilometre Array Pathfinder and Australia Telescope Compact Array are part of the Australia Telescope National Facility, which is managed by CSIRO. Operation of ASKAP is funded by the Australian Government with support from the National Collaborative Research Infrastructure Strategy. ASKAP uses the resources of the Pawsey Supercomputing Centre. Establishment of ASKAP, the Murchison Radio-astronomy Observatory and the Pawsey Supercomputing Centre are initiatives of the Australian Government, with support from the Government of Western Australia and the Science and Industry Endowment Fund. We acknowledge the Wajarri Yamatji as the traditional owners of the Murchison Radio-astronomy Observatory site. The National Radio Astronomy Observatory is a facility of the National Science Foundation operated under cooperative agreement by Associated Universities, Inc. Spectra were obtained at the W.M. Keck Observatory, which is operated as a scientific partnership among Caltech, the University of California, and the National Aeronautics and Space Administration (NASA). The Keck Observatory was made possible by the generous financial support of the W.M. Keck Foundation.

The authors recognize and acknowledge the very significant cultural role and reverence that the summit of Maunakea has always had within the indigenous Hawaiian community. We are most fortunate to have the opportunity to conduct observations from this mountain. This Letter includes data gathered with the 6.5 m *Magellan* Telescopes located at Las Campanas Observatory, Chile, as part of program CN2019A-36. This work makes use of observations from the LCOGT network obtained as part of programs CN2019A-39/CLN2019A-002 and CN2019B-93/CLN2019B-001. The Gemini-S/GMOS observations were carried out as part of program GS-2018B-Q-133, obtained at the Gemini Observatory, which is operated by the Association of Universities for Research in Astronomy, Inc., under a cooperative agreement with the NSF on behalf of the Gemini partnership: the National Science Foundation (United States), National Research Council (Canada), CONICYT (Chile), Ministerio de Ciencia, Tecnología e Innovación Productiva (Argentina), Ministério da Ciência, Tecnologia e Inovação (Brazil), and Korea Astronomy and Space Science Institute (Republic of Korea).

Appendix

SED fitting using CIGALE: To estimate the stellar mass, SFRs, and rest-frame colors of the HGs for FRB 180924, FRB 181112, and FRB 190608, we used CIGALE (Noll et al. 2009), a python-based SED fitting software. The SED for the host of FRB 180924 and FRB 181112 are presented in Bannister et al. (2019) and Prochaska et al. (2019) and an SED for the host of FRB 190608 is presented in Figure 4. CIGALE is fed photometric measurements and redshifts and it computes optimal galaxy properties for assumed models of SFH, stellar population, AGN emission, dust attenuation, and dust emission using a Bayesian framework. We mostly rely on optical photometry but include *Wide-field Infrared Survey Explorer* (*WISE*) measurements where available (Table 3). Due to degeneracies in the model parameters, the estimated properties are somewhat poorly constrained i.e., have errors $\gtrsim 0.3$ dex. We use the following modules in CIGALE.

1. SFH: `sfhdelayed`. It is a delayed-exponential SFH with an initial linear increase and subsequent exponential decay. We do not include a burst population and limit the maximum allowed age of the main population to the cosmological time at the galaxy’s redshift. We fix the initial SFR to $0.1 M_{\odot} \text{ yr}^{-1}$. We allow the e-folding time of the SFH to vary but try to limit it such that the CIGALE estimate for the final SFR is consistent with our spectroscopic estimate.
2. Stellar population model: `bc03`. A stellar population model from Bruzual & Charlot (2003). We use a Chabrier initial mass function and the separation between young and old stars is set to 10^7 yr.
3. Dust attenuation: `dustatt_calzleit`. Dust attenuation model from Calzetti et al. (2000) and Leitherer et al. (2002) for the optical and UV wavelengths, respectively. We fix the UV bump centroid to 217.5 nm, its amplitude to 1.3 and set its FWHM to 35.6 nm. We also set the index of the power law (δ) modifying the attenuation curve to -0.38 .
4. Dust emission: `dale2014`. IR, submillimeter, and radio emission templates from Dale et al. (2014). We allow both the AGN fraction and the template parameter α to vary in our fits. This emission is poorly constrained in the absence of *WISE* measurements.

To estimate the galaxy properties for the host of FRB 190102, the spectra were analyzed with the pPXF package (Cappellari 2017). The spectrum of the FRB 190102 is also presented in Figure 4.

Figure 5 shows a Baldwin, Phillips & Terlevich (BPT) diagram (Baldwin et al. 1981) of the galaxy distribution for two nebular line ratios, which can be used to determine the dominant source of ionization for the interstellar medium. Only one of the four ASKAP FRB host galaxies (HG 181112) lies close to the region populated by star-forming galaxies, while HG 190102 lies in the “composite” region close to the SF/AGN boundary. The FRB 180924 host lies in the LINER region, where gas may be ionized either by a low-excitation AGN or by a population of post-AGB stars (Yan & Blanton 2012). Interestingly, the host of

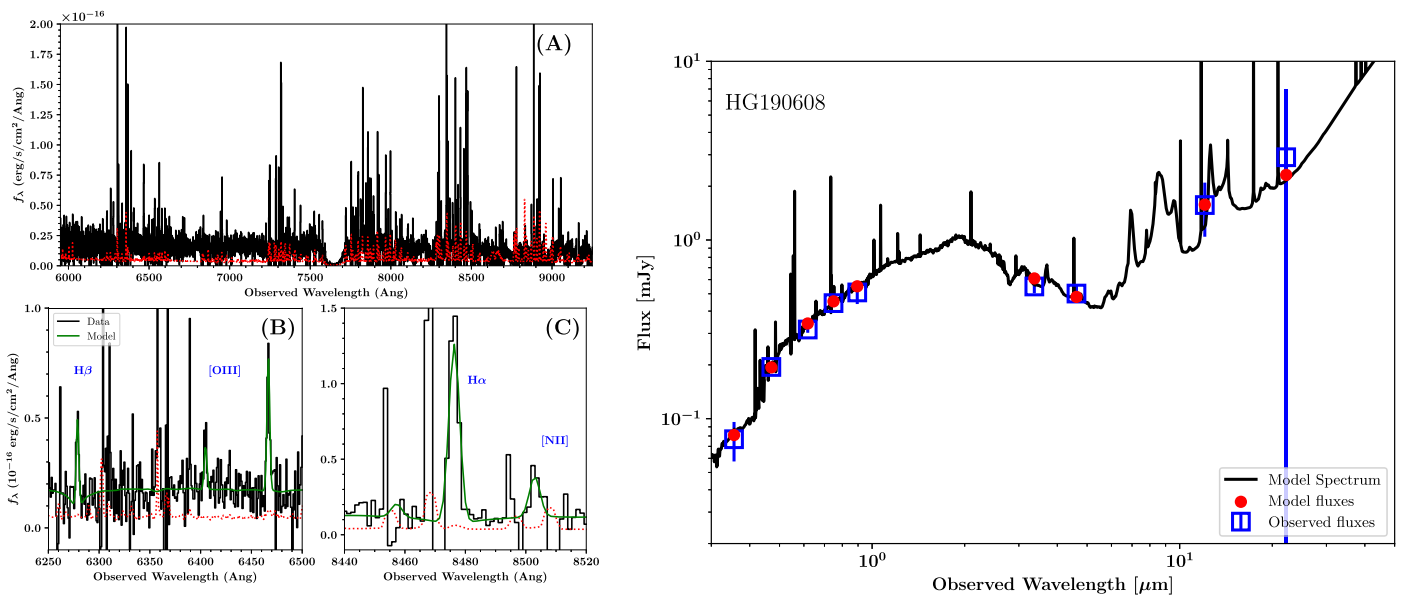


Figure 4. Left panel: spectrum of the host galaxy of FRB 190102. Right panel: SED for the host of FRB 190608.

Table 3
Photometric Details for ASKAP-Localized Host Galaxies

DES					WISE				VLT		LCOGT		
<i>g</i>	<i>r</i>	<i>i</i>	<i>z</i>	<i>Y</i>	<i>W1</i>	<i>W2</i>	<i>W3</i>	<i>W4</i>	<i>g</i>	<i>I</i>	<i>g</i>	<i>r</i>	<i>i</i>
21.62(3)	20.54(2)	20.14(2)	19.85(2)	19.81(6)	16.85(10)	16.06(18)	11.69(-)	8.50(-)	21.38(4)	20.10(2)	21.59(12)	20.46(8)	20.20(11)
22.71(9)	21.73(5)	21.49(6)	21.45(11)	21.07(17)	22.57(4)	21.51(4)	22.37(33)	21.61(22)	21.29(26)

(a) Photometry for HG180924 and HG181112, respectively

VLT				LCOGT		
<i>u</i>	<i>g</i>	<i>I</i>	<i>z</i>	<i>g</i>	<i>r</i>	<i>i</i>
23.7(2)	22.6(1)	21.10(5)	20.8(2)	>22.13	22.06(51)	22.02(73)

(b) Photometry for HG190102

SDSS					LCOGT		
<i>u</i>	<i>g</i>	<i>r</i>	<i>i</i>	<i>z</i>	<i>g</i>	<i>r</i>	<i>i</i>
19.19(9)	18.18(2)	17.65(1)	17.28(2)	17.13(5)	18.28(2)	17.38(1)	17.55(2)

(c) Photometry for HG190608

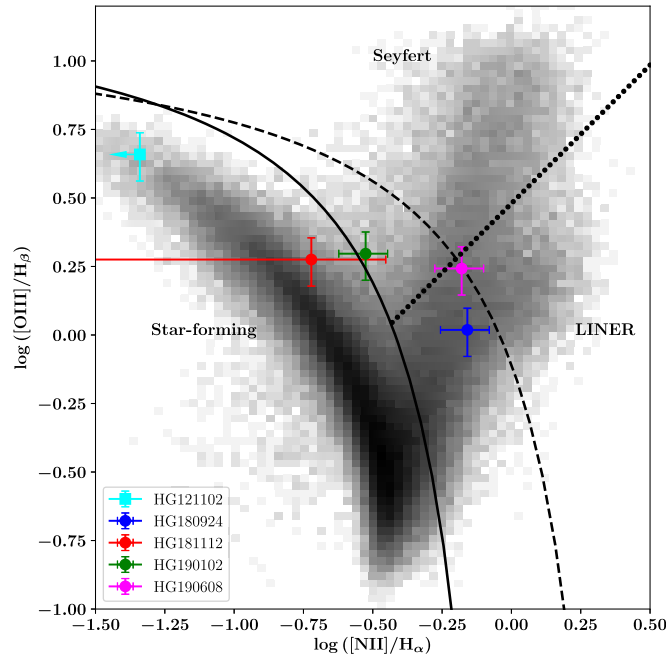


Figure 5. Baldwin et al. (1981) diagnostic plot showing emission line ratios for FRB host galaxies (abbreviated to HG). The background data points show the distribution of $\sim 75,000$ nearby ($0.02 < z < 0.4$) emission-line galaxies from the SDSS, restricted to have $S/N > 5$. Black lines separate the star-forming galaxies (solid) from sources dominated by hard spectra (dashed), and the dotted line separates sources designated as AGNs into either Seyfert or LINER galaxies.

Table 4
Radio Follow-up Observations of the HGs of ASKAP-Localized FRBs

FRB	Telescope	Band (GHz)	T_{start} (UTC)	T_{obs} (s)	$T_{\text{start}} - T_{\text{FRB}}$ (dd:hh:mm:ss)	Resolution (NS \times EW)	rms noise ($\mu\text{Jy}/\text{beam}$)
180924	ATCA-6A	4.5–8.5	2018 Oct 4-12:09:44	15300	009:19:46:33	$8'' \times 2''$	7
181112	ATCA-6B	4.5–8.5	2018 Nov 17-02:47:04	34200	004:09:15:50	$3'' \times 2''$	5
190102	ATCA-1.5D	4.5–8.5	2019 Jan 10-12:21:14	21600	008:06:42:32	$5'' \times 2''$	10
	ATCA-1.5D	4.5–8.5	2019 Jan 14-05:43:24	22320	012:00:04:42	$4'' \times 2''$	10
190608	ATCA-6A	4.5–8.5	2019 Jun 16:13:43:35	9000	017:14:55:22	$20'' \times 2''$	15
	VLA-A	4.0–8.0	2019 Aug 25:05:40:54	3036	077:06:52:41	$1'' \times 1''$	3.5

Table 5

Optical Follow-up Observations of the Host Galaxy of FRB 180924; $T_{\text{FRB}} = 2018$ September 24-16:23:12, FRB 181112; $T_{\text{FRB}} = 2018$ November 12-17:31:15, FRB 190102; $T_{\text{FRB}} = 2019$ January 2-05:38:43 and FRB 190608; $T_{\text{FRB}} = 2019$ June 8-22:48:13. T_{obs} is the Length of Observation, with Multiple Exposures Signified by a Multiplication

Telescope	Instrument	Observation Mode	Band	Effective Wavelength (10^{-3}m)	T_{start} (UTC)	T_{obs} (s)	$T_{\text{start}} - T_{\text{FRB}}$ (dd:hh:mm:ss)
<i>Host of FRB 180924</i>							
Keck	KCWI	IFU	Optical	350–550	2018 Oct 4	4×600	10
Gemini-S	GMOS	Spectroscopy	Optical	470–930	2018 Oct 5-02:15:48	4×700	010:09:52:36
VLT	MUSE	IFU	Optical	475–930	2018 Nov 5	4×628	41
VLT	FORS2	Imaging	<i>g</i>	470	2018 Nov 9-01:02:49	5×500	045:08:39:36
VLT	FORS2	Imaging	<i>I</i>	768	2018 Nov 9-01:48:09	5×90	045:09:24:56
LCOGT-1 m	Sinistro	Imaging	<i>i</i>	754.5	2019 May 31-15:38:14	6×60	248:23:15:02
LCOGT-1 m	Sinistro	Imaging	<i>r</i>	621.5	2019 May 31-15:48:36	10×60	248:23:25:24
LCOGT-1 m	Sinistro	Imaging	<i>g</i>	477	2019 May 31-16:03:20	10×60	248:23:40:08
VLT	X-Shooter	Imaging	<i>g</i>	477	2019 Aug 21-04:39:36	9×300	330:10:52:38
VLT	X-Shooter	Imaging	<i>I</i>	806	2019 Aug 21-05:23:44	9×120	330:11:39:36
VLT	FORS2	Imaging	<i>g</i>	470	2019 Aug 23-04:21:33	5×500	332:11:58:21
VLT	FORS2	Imaging	<i>I</i>	768	2018 Aug 23-05:29:19	5×90	332:13:06:07
<i>Host of FRB 181112</i>							
VLT	FORS2	Imaging	<i>g</i>	470	2018 Dec 3-01:34:13	5×500	020:08:02:59
VLT	FORS2	Imaging	<i>I</i>	768	2018 Dec 3-02:10:12	5×90	020:08:38:57
LCOGT-1 m	Sinistro	Imaging	<i>i</i>	754.5	2019 May 31-19:10:42	10×60	200:01:39:27
LCOGT-1 m	Sinistro	Imaging	<i>r</i>	621.5	2019 May 31-19:25:25	10×60	200:01:54:10



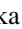



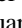








Table 5
(Continued)

Telescope	Instrument	Observation Mode	Band	Effective Wavelength (10^{-9} m)	T_{start} (UTC)	T_{obs} (s)	$T_{\text{start}} - T_{\text{FRB}}$ (dd:hh:mm:ss)
LCOGT-1 m	Sinistro	Imaging	<i>g</i>	477	2019 May 31-19:40:09	10×60	200:02:08:54
VLT	X-Shooter	Imaging	<i>g</i>	477	2019 Aug 21-02:02:56	9×300	281:08:31:41
VLT	X-Shooter	Imaging	<i>l</i>	806	2019 Aug 21-02:50:01	9×120	281:09:18:46
VLT	FORS2	Imaging	<i>g</i>	470	2019 Aug 23-04:08:18	5×500	283:10:37:03
VLT	FORS2	Imaging	<i>l</i>	768	2019 Aug 23-04:42:16	5×90	283:11:11:01
<i>Host of FRB 190102</i>							
VLT	FORS2	Imaging	<i>l</i>	768	2019 Jan 12-01:14:23	5×90	009:19:35:41
VLT	FORS2	Imaging	<i>g</i>	470	2019 Jan 12-01:25:48	3×500	009:19:47:06
Magellan	MagE	Spectroscopy	Optical	320–900	2019 Mar 12-08:36:03	1×3700	069:02:57:20
LCOGT-1 m	Sinistro	Imaging	<i>i</i>	754.5	2019 May 31-16:39:09	11×60	149:11:00:26
LCOGT-1 m	Sinistro	Imaging	<i>g</i>	477	2019 May 31-17:16:01	10×60	149:11:37:18
LCOGT-1 m	Sinistro	Imaging	<i>r</i>	621.5	2019 May 31-17:30:44	10×60	149:11:52:01
VLT	FORS2	Imaging	<i>g</i>	470	2019 Jun 2-05:43:05	4×500	151:00:04:22
VLT	FORS2	Imaging	<i>u</i>	361	2019 Jun 17-09:19:36	5×560	166:03:40:54
VLT	FORS2	Imaging	<i>z</i>	910	2019 Jun 17-10:09:45	5×30	166:04:31:03
VLT	X-Shooter	Imaging	<i>g</i>	477	2019 Aug 21-05:51:53	9×300	231:00:13:10
VLT	X-Shooter	Imaging	<i>l</i>	806	2019 Aug 21-06:39:02	9×120	231:01:00:19
VLT	FORS2	Imaging	<i>l</i>	768	2019 Aug 23-03:55:01	5×90	232:22:16:18
VLT	FORS2	Imaging	<i>g</i>	470	2019 Aug 23-07:19:27	5×500	233:01:40:44
VLT	FORS2	Imaging	<i>u</i>	361	2019 Nov 20-01:25:38	5×560	321:19:36:55
<i>Host of FRB 190608</i>							
LCOGT-1 m	Sinistro	Imaging	<i>i</i>	754.5	2019 Jun 9-03:05:10	10×60	00:04:16:57
LCOGT-1 m	Sinistro	Imaging	<i>g</i>	477	2019 Jun 9-03:19:52	10×60	00:04:31:39
LCOGT-1 m	Sinistro	Imaging	<i>r</i>	621.5	2019 Jun 9-03:34:34	10×60	00:04:46:21
VLT	X-Shooter	Imaging	<i>g</i>	477	2019 Aug 21-04:39:36	8×300	073:05:51:23
VLT	X-Shooter	Imaging	<i>l</i>	806	2019 Aug 21-05:23:44	8×120	073:06:35:31

FRB 190608 lies at the boundary of Seyfert and LINER. It is a known Type 1 AGN (i.e., Seyfert) as noted before. Thus the four ASKAP host galaxies show a diversity of ionization properties, rather than being drawn from a population of purely star-forming systems. For further comparison, we include measurements from the host of FRB 121102, which lies in the star-forming population.

The details of the radio and optical follow-up observations for the hosts of ASKAP-localized FRBs are listed in Tables 4 and 5, respectively.

ORCID iDs

Shivani Bhandari  <https://orcid.org/0000-0003-3460-506X>
 Elaine M. Sadler  <https://orcid.org/0000-0002-1136-2555>
 J. Xavier Prochaska  <https://orcid.org/0000-0002-7738-6875>
 Stuart D. Ryder  <https://orcid.org/0000-0003-4501-8100>
 Lachlan Marnoch  <https://orcid.org/0000-0003-1483-0147>
 Keith W. Bannister  <https://orcid.org/0000-0003-2149-0363>
 Jean-Pierre Macquart  <https://orcid.org/0000-0001-6763-8234>
 Chris Flynn  <https://orcid.org/0000-0002-4796-745X>
 Ryan M. Shannon  <https://orcid.org/0000-0002-7285-6348>
 Nicolas Tejos  <https://orcid.org/0000-0002-1883-4252>
 Cherie K. Day  <https://orcid.org/0000-0002-8101-3027>
 Adam T. Deller  <https://orcid.org/0000-0001-9434-3837>
 Ron Ekers  <https://orcid.org/0000-0002-3532-9928>
 Sebastian Lopez  <https://orcid.org/0000-0003-0389-0902>
 Elizabeth K. Mahony  <https://orcid.org/0000-0002-5053-2828>

References

Abbott, T. M. C., Abdalla, F. B., Allam, S., et al. 2018, *ApJS*, 239, 18
 Agarwal, D., Lorimer, D. R., Fialkov, A., et al. 2019, *MNRAS*, 490, 1

Ahn, C. P., Alexandroff, R., Allende Prieto, C., et al. 2012, *ApJS*, 203, 21
 Alam, S., Albareti, F. D., Allende Prieto, C., et al. 2015, *ApJS*, 219, 12
 Amiri, M., Bandura, K., Bhardwaj, M., et al. 2019, *Natur*, 566, 230
 Appenzeller, I., Fricke, K., Fürtig, W., et al. 1998, *Msngr*, 94, 1
 Artale, M. C., Mapelli, M., Giacobbo, N., et al. 2019, *MNRAS*, 487, 1675
 Bacon, R., Accardo, M., Adjali, L., et al. 2010, *Proc. SPIE*, 7735, 773508
 Baldwin, J. A., Phillips, M. M., & Terlevich, R. 1981, *PASP*, 93, 5
 Bannister, K. W., Deller, A. T., Phillips, C., et al. 2019, *Sci*, 365, 6453
 Bannister, K. W., Shannon, R. M., Macquart, J.-P., et al. 2017, *ApJL*, 841, L12
 Bertin, E., & Arnouts, S. 1996, *A&AS*, 117, 393
 Bhandari, S., Bannister, K. W., James, C. W., et al. 2019, *MNRAS*, 486, 70
 Blanton, M. R., Bershad, M. A., Abolfathi, B., et al. 2017, *AJ*, 154, 28
 Brinchmann, J., Charlot, S., Heckman, T. M., et al. 2004, arXiv:astro-ph/0406220
 Brown, T. M., Baliber, N., Bianco, F. B., et al. 2013, *PASP*, 125, 1031
 Bruzual, G., & Charlot, S. 2003, *MNRAS*, 344, 1000
 Cai, Y.-F., Sabancilar, E., Steer, D. A., & Vachaspati, T. 2012, *PhRvD*, 86, 043521
 Calzetti, D., Armus, L., Bohlin, R. C., et al. 2000, *ApJ*, 533, 682
 Cappellari, M. 2017, *MNRAS*, 466, 798
 Chatterjee, S., Law, C. J., Wharton, R. S., et al. 2017, *Natur*, 541, 58
 CHIME/FRB Collaboration, Andersen, B., Bandura, K., et al. 2019, *ApJL*, 885, L24
 Connor, L. 2019, *MNRAS*, 487, 5753
 Connor, L., Sievers, J., & Pen, U.-L. 2016, *MNRAS*, 458, L19
 Cordes, J., & Wasserman, I. 2016, *MNRAS*, 457, 232
 Cordes, J. M., & Chatterjee, S. 2019, *ARA&A*, 57, 417
 Craig, M., Crawford, S., Seifert, M., et al. 2017, *astropy/ccdproc*: v1.3.0.post1, Zenodo, doi:10.5281/ZENODO.1069648
 Dale, D. A., Helou, G., Magdis, G., et al. 2014, AAS Meeting, 223, 453.01
 Falcke, H., & Rezzolla, L. 2014, *A&A*, 562, A137
 Farah, W., Flynn, C., Bailes, M., et al. 2019, *MNRAS*, 488, 2989
 Freudling, W., Romaniello, M., Bramich, D. M., et al. 2013, *A&A*, 559, 96
 Fruchter, A. S., Levan, A. J., Strolger, L., et al. 2006, *Natur*, 441, 463
 Hook, I. M., Jørgensen, I., Allington-Smith, J. R., et al. 2004, *PASP*, 116, 425
 Jacob, J. C., Katz, D. S., Berriman, G. B., et al. 2010, *Montage: An Astronomical Image Mosaicking Toolkit*, Astrophysics Source Code Library, ascl:1010.036
 James, C. W. 2019, *MNRAS*, 486, 5934
 Kashiyama, K., Ioka, K., & Mészáros, P. 2013, *ApJL*, 776, L39

- Kelly, P. L., & Kirshner, R. P. 2012, *ApJ*, 759, 107
- Kumar, P., Shannon, R., Osłowski, S., et al. 2019, *ApJL*, 887, L30
- Leitherer, C., Li, I. H., Calzetti, D., & Heckman, T. M. 2002, *ApJS*, 140, 303
- Levan, A. J., Wynn, G. A., Chapman, R., et al. 2006, *MNRAS*, 368, L1
- Li, L.-B., Huang, Y.-F., Geng, J.-J., & Li, B. 2018, *RAA*, 18, 061
- Lingam, M., & Loeb, A. 2017, *ApJL*, 837, L23
- Lorimer, D. R., Bailes, M., McLaughlin, M. A., Narkevic, D. J., & Crawford, F. 2007, *Sci*, 318, 777
- Macquart, J.-P., Bailes, M., Bhat, N. D. R., et al. 2010, *PASA*, 27, 272
- Macquart, J.-P., & Johnston, S. 2015, *MNRAS*, 451, 3278
- Macquart, J. P., Shannon, R. M., Bannister, K. W., et al. 2019, *ApJL*, 872, L19
- Macquart, J.-P., Prochaska, J. X., McQuinn, M., et al. 2020, *Natur*, submitted
- Margalit, B., Berger, E., & Metzger, B. D. 2019, *ApJ*, 886, 110
- Margalit, B., & Metzger, B. D. 2018, *ApJL*, 868, L4
- Marshall, J. L., Burles, S., Thompson, I. B., et al. 2008, *Proc. SPIE*, 7014, 701454
- Martin, D. C., Wyder, T. K., Schiminovich, D., et al. 2007, *ApJS*, 173, 342
- Masui, K., Lin, H.-H., Sievers, J., et al. 2015, *Natur*, 528, 523
- Metzger, B. D., Berger, E., & Margalit, B. 2017, *ApJ*, 841, 14
- Morrissey, P., Matuszewski, M., Martin, D. C., et al. 2018, *ApJ*, 864, 93
- Moustakas, J., Coil, A. L., Aird, J., et al. 2013, *ApJ*, 767, 50
- Noll, S., Burgarella, D., Giovannoli, E., et al. 2009, *A&A*, 507, 1793
- Pen, U.-L., & Connor, L. 2015, *ApJ*, 807, 179
- Perley, D. A., Quimby, R. M., Yan, L., et al. 2016, *ApJ*, 830, 13
- Piro, A. L. 2016, *ApJL*, 824, L32
- Platts, E., Weltman, A., Walters, A., et al. 2018, arXiv:1810.05836
- Popov, S. B., & Postnov, K. A. 2010, in Proc. Conf. Evolution of Cosmic Objects through their Physical Activity, ed. H. A. Harutyunian, A. M. Mickaelian, & Y. Terzian (Yerevan: Gitutyun Publishing House of NAS RA), 129
- Prochaska, J. X., Macquart, J.-P., McQuinn, M., et al. 2019, *Sci*, 366, 6462
- Qiu, H., Bannister, K. W., Shannon, R. M., et al. 2019, *MNRAS*, 486, 166
- Ravi, V., Catha, M., D'Addario, L., et al. 2019, *Natur*, 572, 352
- Schlafly, E. F., & Finkbeiner, D. P. 2011, *ApJ*, 737, 103
- Shannon, R. M., Macquart, J.-P., Bannister, K. W., et al. 2018, *Natur*, 562, 386
- Spitler, L., Scholz, P., Hessels, J., et al. 2016, *Natur*, 531, 202
- Spitler, L. G., Cordes, J. M., Hessels, J. W. T., et al. 2014, *ApJ*, 790, 101
- Stern, J., & Laor, A. 2012, *MNRAS*, 423, 600
- Strateva, I., Ivezić, Ž., Knapp, G. R., et al. 2001, *ApJ*, 122, 1861
- Sullivan, M., Mobasher, B., Chan, B., et al. 2001, *ApJ*, 558, 72
- Tendulkar, S. P., Bassa, C. G., Cordes, J. M., et al. 2017, *ApJL*, 834, L7
- Totani, T. 2013, *PASJ*, 65, L12
- Vernet, J., Dekker, H., D'Odorico, S., et al. 2011, *A&A*, 536, A105
- Vieyro, F. L., Romero, G. E., Bosch-Ramon, V., Marcote, B., & del Valle, M. V. 2017, *A&A*, 602, A64
- Wolf, R. C., D'Andrea, C. B., Gupta, R. R., et al. 2016, *ApJ*, 821, 115
- Yamasaki, S., Totani, T., & Kiuchi, K. 2018, *PASJ*, 70, 39
- Yan, R., & Blanton, M. R. 2012, *ApJ*, 747, 61
- Zadorozhna, L. V. 2015, *AASP*, 5, 43
- Zhang, B. 2017, *ApJL*, 836, L32